Effective quantum dynamics induced by a driven two-level-system bath

Katja Kustura,* Oriol Romero-Isart, and Carlos Gonzalez-Ballestero
Institute for Quantum Optics and Quantum Information, Austrian Academy of Sciences, 6020 Innsbruck, Austria and Institute for Theoretical Physics, University of Innsbruck, 6020 Innsbruck, Austria

(Received 21 December 2020; accepted 10 May 2021; published 24 May 2021)

We derive a Born-Markov master equation describing the dissipation induced by a bath of lossy but coherently driven two-level systems (TLSs) coupled to a bosonic system via Jaynes-Cummings interaction. We analytically derive all the master-equation rates. We characterize these rates for the particular case of a single-mode system coupled to identical TLSs. We study the steady state of the system and its exotic properties stemming from the nonthermal stationary state of the driven TLS bath. These properties include dissipative amplification, bath-induced linear instability, and both coherent and dissipative squeezing. The master equation is valid for arbitrarily strong TLS driving and it can be generalized to include multilevel systems or other system-bath interaction terms, among others. Our work provides a tool to study and characterize TLS-induced decoherence, a key limiting factor in quantum technological devices based on, for instance, superconducting circuits, magnonic systems, or quantum acoustics.

DOI: 10.1103/PhysRevA.103.053709

I. INTRODUCTION

Two-level impurities are known to limit the coherence of many systems of both fundamental and technological interest ranging from superconducting qubits [1–5] and resonators [6–8] to electronic transistors [9,10], ion traps [11], solid-state quantum emitters [12,13], and acoustic [14–16] and magnonic platforms [17–22]. This two-level-system (TLS)–induced decoherence becomes especially significant at low temperature where additional bosonic baths are depleted [17]. Recent advances in the control of quantum technological platforms have sparked a revived interest in probing and controlling these TLS baths, whose impact can now be accurately measured [17] and even suppressed [14,15]. An important step toward this goal would be to bridge the gap between the current, platform-dependent, solid-state-based theoretical descriptions of TLS-induced dissipation, such as the standard tunneling model [1,8,23–26], and the general quantum-mechanical formulation of dissipation widely used in quantum optics. Specifically, the derivation of a master equation describing the decoherence induced by TLS baths is timely.

Any description of the dissipation discussed above must account for two unconventional aspects: first, the two-level statistics of the bath, whose richer phenomenology in comparison with, e.g., bosonic baths [27] makes them the focus of intense research [28–30], and second, and more importantly, the possibility that the TLSs forming the bath are subject not only to their intrinsic loss but also to coherent driving, which drives the bath out of thermal equilibrium. As a consequence, the standard assumption in open quantum systems, namely, a bath in thermal equilibrium, does not apply. Not only can TLS baths be subject to purposeful driving [14,15], but, generally, driving the system will unavoidably result in driving of the bath, either through direct interaction with the driving fields or indirectly through the action of the system itself [31–33]. This spurious bath driving can be strong and have important consequences on the system dynamics and response, especially for nanostructures [31–33]. In this paper we derive a Born-Markov master equation describing the open dynamics of a bosonic system in contact with a bath of independent TLS subject to arbitrarily strong coherent driving. We demonstrate the rich system phenomenology arising both from the TLS statistics and from the nonthermal stationary state of the bath, including amplification, steady-state squeezing, and dynamical instabilities for typical parameters in, for instance, microwave cavities. All these features evidence the potential of controllable TLS bath driving as a tool to reduce TLS-induced decoherence and to probe and understand the complex properties of TLS baths [14].

Our paper is organized as follows. We start in Sec. II by describing the model and outlining the derivation of the master equation for the system. In Sec. III we focus on the particular case of a single-mode system coupled to a bath of identical TLSs. We characterize the behavior of the master-equation rates and the system steady state, focusing on the effects arising from the nonthermal state of the TLS bath. The conclusions and outlook are provided in Sec. IV.

II. MODEL AND MASTER-EQUATION DERIVATION

In this section we describe the derivation of the master equation for the system interacting with a driven TLS bath. We start in Sec. II A by introducing the parameters and the assumptions of our model. We then proceed in Sec. II B to give a summary of the master-equation derivation under the Born-Markov approximation.

*katja.kustura@uibk.ac.at

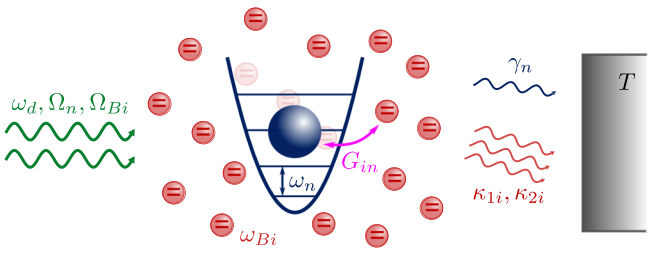

FIG. 1. Scheme of the model. A set of N_b bosonic modes (here depicted as one for simplicity) with frequencies ω_n and decay rates γ_n $(n = 1, \ldots, N_b)$ is coupled to a bath composed of N two-level systems with frequencies ω_{Bi} and decay and dephasing rates κ_{1i} and κ_{2i}, respectively $(i = 1, \ldots, N)$. The nth system mode is coupled to the ith TLS at a rate G_{in}. Both the system and bath are coherently driven at frequency ω_d and with respective amplitudes Ω_n and Ω_{Bi}.

A. Description of the model

The system under study, schematically shown in Fig. 1, consists of an ensemble of N_b independent bosonic modes with frequencies ω_n $(n = 1, 2, \ldots, N_b)$, each coupled to a finite bath of N noninteracting TLSs with frequencies ω_{Bi} $(i = 1, 2, \ldots, N)$. Both the system and the TLS bath are open, i.e., coupled to independent external reservoirs which we model as usual thermal baths at temperature T. Additionally, both the system and the TLS bath are subject to coherent driving. The dynamics of the total system are given by the Liouville–von Neumann equation

$$\dot{\hat{\rho}}_{\text{tot}} = (\mathcal{L}_S + \mathcal{L}_B + \mathcal{L}_I)[\hat{\rho}_{\text{tot}}], \tag{1}$$

where $\hat{\rho}_{\text{tot}}$ is the total density matrix of the system and the bath and $\mathcal{L}_S$, $\mathcal{L}_B$, and $\mathcal{L}_I$ are the Liouvillian superoperators [27] denoting the system, the bath, and the interaction parts, respectively. Let us describe each term separately.

The system Liouvillian $\mathcal{L}_S$ acts only on the system Hilbert space and is given by the standard optical master equation [27]

$$\mathcal{L}_S[\hat{\rho}] = -\frac{i}{\hbar}[\hat{H}_S, \hat{\rho}] + \mathcal{S}[\hat{\rho}]. \tag{2}$$

The first term describes the coherent dynamics of the externally driven ensemble of bosonic modes through the Hamiltonian

$$\hat{H}_S = \hbar \sum_{n=1}^{N_b} \{\omega_n \hat{s}_n^\dagger \hat{s}_n + (\Omega_n \hat{s}_n e^{i\omega_d t} + \text{H.c.})\}. \tag{3}$$

Here $\Omega_n \in \mathbb{C}$ is the driving rate for mode n, ω_d is the driving frequency, and $\hat{s}_n$ and $\hat{s}_n^\dagger$ are bosonic annihilation and creation operators, respectively, obeying the commutation relations $[\hat{s}_m, \hat{s}_n] = [\hat{s}_m^\dagger, \hat{s}_n^\dagger] = 0$ and $[\hat{s}_m, \hat{s}_n^\dagger] = \delta_{mn}$. The second term in Eq. (2) describes the incoherent dynamics induced by the thermal bath and is given by

$$\mathcal{S}[\hat{\rho}] = \sum_{n=1}^{N_b} \gamma_n \left\{[1 + \bar{n}(\omega_n)]\mathcal{D}_{\hat{s}_n, \hat{s}_n^\dagger}[\hat{\rho}] + \bar{n}(\omega_n)\mathcal{D}_{\hat{s}_n^\dagger, \hat{s}_n}[\hat{\rho}]\right\}, \tag{4}$$

where γ_n is the decay rate of a mode n, $\mathcal{D}_{\hat{a},\hat{b}}[\hat{\rho}] = \hat{a}\hat{\rho}\hat{b} - \{\hat{b}\hat{a}, \hat{\rho}\}/2$ is the Lindblad superoperator, and $\bar{n}(\omega) = [\exp(\hbar\omega/k_B T) - 1]^{-1}$ is the Bose-Einstein distribution, with k_B the Boltzmann constant.

The bath contribution $\mathcal{L}_B$ acts only on the Hilbert space of the TLS and is given by the standard Bloch master equation [27]

$$\mathcal{L}_B[\hat{\rho}] = -\frac{i}{\hbar}[\hat{H}_B, \hat{\rho}] + \mathcal{B}[\hat{\rho}]. \tag{5}$$

The first term describes the coherent dynamics of externally driven TLSs through the Hamiltonian

$$\hat{H}_B = \frac{\hbar}{2} \sum_{i=1}^{N} \{\omega_{Bi}\hat{\sigma}_{zi} + (\Omega_{Bi}\hat{\sigma}_{+i}e^{-i\omega_d t} + \text{H.c.})\}. \tag{6}$$

Here $\Omega_{Bi} \in \mathbb{C}$ is the driving rate for emitter i and we define $\hat{\sigma}_{\pm i} = (\hat{\sigma}_{xi} \pm i\hat{\sigma}_{yi})/2$ in terms of the spin-$\frac{1}{2}$ Pauli operators $\{\hat{\sigma}_{xi}, \hat{\sigma}_{yi}, \hat{\sigma}_{zi}\}$, which obey the commutation relations $[\hat{\sigma}_{\alpha i}, \hat{\sigma}_{\beta j}] = i\delta_{ij}\epsilon_{\alpha\beta\gamma}\hat{\sigma}_{\gamma i}$ for $\alpha, \beta, \gamma = x, y, z$, with $\epsilon_{\alpha\beta\gamma}$ the Levi-Cività tensor. The second term in Eq. (5) describes the incoherent TLS dynamics induced by the thermal bath and is given by

$$\mathcal{B}[\hat{\rho}] = \sum_{i=1}^{N} \big\{\kappa_{1i}[1 + \bar{n}(\omega_{Bi})]\mathcal{D}_{\hat{\sigma}_{-i}, \hat{\sigma}_{+i}}[\hat{\rho}] + \kappa_{1i}\bar{n}(\omega_{Bi})\mathcal{D}_{\hat{\sigma}_{+i}, \hat{\sigma}_{-i}}[\hat{\rho}] + \kappa_{2i}\mathcal{D}_{\hat{\sigma}_{zi}, \hat{\sigma}_{zi}}[\hat{\rho}]\big\}. \tag{7}$$

The terms proportional to κ_{1i} describe decay and absorption, whereas the term proportional to κ_{2i} describes dephasing. It is useful for the following discussion to define a single decoherence timescale including both processes, namely, the TLS transverse decay rate, as

$$\kappa_{ti} = \frac{\kappa_{1i}}{2}[1 + 2\bar{n}(\omega_{Bi})] + 2\kappa_{2i}. \tag{8}$$

Finally, the interaction part of the Liouvillian describes the coupling between the system of bosonic modes and the TLS bath. We assume a standard Jaynes-Cummings interaction, which, as discussed below, is appropriate to discuss many physical scenarios of interest. Specifically,

$$\mathcal{L}_I[\hat{\rho}] = -\frac{i}{\hbar}[\hat{V}, \hat{\rho}] = -\frac{i}{\hbar}\sum_{ni}[G_{in}\hat{\sigma}_{+i}\hat{s}_n + \text{H.c.}, \hat{\rho}], \tag{9}$$

with G_{in} the coupling rate between the ith TLS and the nth bosonic system mode. In Eq. (9) and hereafter, we omit for simplicity the upper limit of the sums in i and n, namely, N and N_b, respectively.

The choice of the above specific forms for the Liouvillians is physically motivated, especially by applications in microwave and magnonic technologies [1–8,17–22]. When applied to these systems, the bosonic modes $\hat{s}_n$ represent electromagnetic degrees of freedom, and our model recovers the usual cavity quantum electrodynamics description under the rotating-wave and independent TLS approximation [34,35]. In other words, our model is appropriate to describe these systems provided the validity conditions for the rotating-wave approximation are fulfilled both for the coherent driving and for the system-TLS interaction terms, namely, $|\omega_n - \omega_d| \ll \omega_n + \omega_d$, $|\omega_{Bi} - \omega_d| \ll \omega_{Bi} + \omega_d$, $|\omega_n - \omega_{Bi}| \ll \omega_n + \omega_{Bi}$, $|G_{in}| \ll \omega_n + \omega_{Bi}$, $|\Omega_n| \ll \omega_n + \omega_d$, and $|\Omega_{Bi}| \ll \omega_{Bi} + \omega_d$. Although these conditions are usually fulfilled, the rotating-wave approximation could break down, e.g., in strongly coupled systems [34,35]. Similarly,

the independent TLS approximation, namely, neglecting any direct (e.g., dipole-dipole) coupling between the TLSs, is also well justified since the TLS densities in these systems are typically sufficiently small. Finally, in these platforms the drivings of the system and the TLS usually have the same frequency ω_d, as they originate from the same microwave signal. For all the above reasons, our model can be directly applied to most microwave and magnonic platforms.

B. Born-Markov master equation

Our aim is to trace out the TLS degrees of freedom and obtain an effective equation of motion for the bosonic system. First, we transform the Liouville–von Neumann equation (1) to a frame rotating at the driving frequency ω_d, by applying the unitary transformation

$$\hat{U}_1(t) = \exp\left[i\omega_d t\left(\sum_n \hat{s}_n^\dagger \hat{s}_n + \sum_i \frac{\hat{\sigma}_{zi}}{2}\right)\right]. \tag{10}$$

The Liouville–von Neumann equation in the rotating frame is

$$\dot{\hat{\rho}}_{\rm tot}^{(1)} = \left(\mathcal{L}_S^{(1)} + \mathcal{L}_B^{(1)} + \mathcal{L}_I^{(1)}\right)\left[\hat{\rho}_{\rm tot}^{(1)}\right], \tag{11}$$

with $\hat{\rho}_{\rm tot}^{(1)}(t) = \hat{U}_1(t)\hat{\rho}_{\rm tot}(t)\hat{U}_1^\dagger(t)$ and time-independent Liouvillian superoperators for the system, the bath, and the interaction part given as $\mathcal{L}_S^{(1)}$, $\mathcal{L}_B^{(1)}$, and $\mathcal{L}_I^{(1)}$, respectively. These three Liouvillians have the same form as Eqs. (2), (5), and (9) with modified time-independent system and bath Hamiltonians given by

$$\hat{H}_S^{(1)} = \hbar\sum_n \{\Delta_n \hat{s}_n^\dagger \hat{s}_n + (\Omega_n \hat{s}_n + \text{H.c.})\}, \tag{12}$$

$$\hat{H}_B^{(1)} = \frac{\hbar}{2}\sum_i \{\Delta_{Bi}\hat{\sigma}_{zi} + (\Omega_{Bi}\hat{\sigma}_{+i} + \text{H.c.})\}, \tag{13}$$

respectively, with $\Delta_n = \omega_n - \omega_d$ and $\Delta_{Bi} = \omega_{Bi} - \omega_d$.

Second, we make the change of variables in the interaction Liouvillian $\mathcal{L}_I^{(1)}$,

$$\hat{\tilde{\sigma}}_{\alpha i}(t) = \hat{\sigma}_{\alpha i} - \langle\hat{\sigma}_{\alpha i}\rangle(t) \quad (\alpha = +, -, z), \tag{14}$$

where $\langle\hat{\sigma}_{\alpha i}\rangle(t) = \text{tr}[\hat{\sigma}_{\alpha i}\hat{\rho}_{\rm tot}^{(1)}(t)]$. From Eq. (9) we obtain an effective system driving term such that Eq. (12) acquires a total time-dependent driving given by the rate

$$\Omega_n'(t) = \Omega_n + \sum_i G_{in}\langle\hat{\sigma}_{+i}\rangle(t). \tag{15}$$

This time-dependent term is typical for driven baths and can be interpreted as an effective force acting on the system [31–33].

Finally, we transform Eq. (11) to a second rotating frame, by applying the unitary transformation

$$\hat{U}_2(t) = \exp\left[it\left(\sum_n \Delta_n \hat{s}_n^\dagger \hat{s}_n + \frac{\hat{H}_B^{(1)}}{\hbar}\right)\right]. \tag{16}$$

The Liouville–von Neumann equation in the second rotating frame is

$$\begin{aligned}\dot{\hat{\rho}}_{\rm tot}^{(2)} &= \left\{\mathcal{L}_S^{(2)}(t) + \mathcal{B}^{(2)}(t) + \mathcal{L}_I^{(2)}(t)\right\}\left[\hat{\rho}_{\rm tot}^{(2)}\right] \\ &\equiv \mathcal{L}^{(2)}(t)\left[\hat{\rho}_{\rm tot}^{(2)}\right],\end{aligned} \tag{17}$$

with $\hat{\rho}_{\rm tot}^{(2)}(t) = \hat{U}_2(t)\hat{\rho}_{\rm tot}^{(1)}(t)\hat{U}_2^\dagger(t)$ and $\mathcal{L}^{(2)}(t)$ denoting the total Liouvillian. Here the system Liouvillian is given by

$$\mathcal{L}_S^{(2)}(t)[\hat{\rho}] = -\frac{i}{\hbar}\sum_n \left[\Omega_n'(t)\hat{s}_n^{(2)}(t) + \text{H.c.}, \hat{\rho}\right] + \mathcal{S}[\hat{\rho}], \tag{18}$$

with $\hat{O}^{(2)}(t) = \hat{U}_2(t)\hat{O}\hat{U}_2^\dagger(t)$. The bath Liouvillian $\mathcal{B}^{(2)}(t)$ maintains the same form as Eq. (7), under the substitution $\hat{\sigma}_{\alpha i} \to \hat{\sigma}_{\alpha i}^{(2)}(t)$. Finally, the interaction Liouvillian reads

$$\begin{aligned}\mathcal{L}_I^{(2)}(t)[\hat{\rho}] &= -\frac{i}{\hbar}[\hat{V}^{(2)}(t), \hat{\rho}] \\ &= -\frac{i}{\hbar}\sum_{ni}\left[G_{in}\hat{\tilde{\sigma}}_{+i}^{(2)}(t)\hat{s}_n^{(2)}(t) + \text{H.c.}, \hat{\rho}\right].\end{aligned} \tag{19}$$

The next step in the master-equation derivation is to trace out the TLS bath in the Born-Markov approximation. Since the standard approach assumes that the system and the bath are closed and this is not our case, we employ a generalized approach based on projection superoperator techniques [27]. We define a projection superoperator $\mathcal{P}$ that acts on the space of density matrices for the compound system and bath as

$$\mathcal{P}\hat{\rho}(t) = \text{tr}_B[\hat{\rho}(t)] \otimes \hat{\rho}_{B,s}^{(2)}(t), \tag{20}$$

where tr_B indicates a partial trace over the bath degrees of freedom and $\hat{\rho}_{B,s}^{(2)}(t)$ denotes the stationary state of the bath Liouvillian, namely,

$$\mathcal{B}^{(2)}(t)\left[\hat{\rho}_{B,s}^{(2)}(t)\right] = \mathcal{L}_B^{(1)}\left[\hat{\rho}_{B,s}^{(1)}\right] = 0, \tag{21}$$

with $\hat{\rho}_{B,s}^{(1)} = \hat{U}_2^\dagger(t)\hat{\rho}_{B,s}^{(2)}(t)\hat{U}_2(t)$. Note that this stationary state of the bath is not thermal due to the presence of driving. The evolution of the projection $\mathcal{P}\hat{\rho}_{\rm tot}^{(2)}(t)$ can be expressed by the Nakajima-Zwanzig equation [27]

$$\begin{aligned}\frac{d}{dt}\mathcal{P}\hat{\rho}_{\rm tot}^{(2)}(t) &= \mathcal{P}\mathcal{L}^{(2)}(t)\mathcal{P}\hat{\rho}_{\rm tot}^{(2)}(t) \\ &\quad + \mathcal{P}\mathcal{L}^{(2)}(t)\int_0^t d\tau\, \mathcal{G}(t,\tau)\mathcal{Q}\mathcal{L}^{(2)}(\tau)\mathcal{P}\hat{\rho}_{\rm tot}^{(2)}(\tau),\end{aligned} \tag{22}$$

where $\mathcal{Q} = 1 - \mathcal{P}$, $\mathcal{G}(t,\tau) = \mathcal{T}_+ \exp[\int_\tau^t d\tau' \mathcal{Q}\mathcal{L}^{(2)}(\tau')]$, with $\mathcal{T}_+$ the time-ordering superoperator, and we assume that the system and bath are uncorrelated at $t = 0$, i.e., $\mathcal{Q}\hat{\rho}_{\rm tot}^{(2)}(0) = 0$. Equation (22) is an exact reformulation of Eq. (17) and it is particularly convenient for two reasons. First, its form allows us to perform the Born-Markov approximation in a simpler fashion (shown below). Second, by taking the trace of Eq. (22) over the bath degrees of freedom, one directly obtains a dynamical equation for the reduced density matrix of the system.

We now simplify Eq. (22) with the Born and Markov approximations. First, we assume that the TLS bath is not significantly affected by its interaction with the system, a condition which is satisfied when the system-bath interaction is weak, namely, $|G_{in}| \ll \kappa_{ti}$. This allows us to undertake the Born approximation

$$\hat{\rho}_{\rm tot}^{(2)}(t) \approx \hat{\rho}_{B,s}^{(2)}(t) \otimes \hat{\rho}_S^{(2)}(t), \tag{23}$$

where the bath stationary state is given by Eq. (21) and $\hat{\rho}_S^{(2)}(t) = \text{tr}_B[\hat{\rho}^{(2)}(t)]$ is the reduced density matrix of the system. Under the Born approximation, the expectation values

of the Pauli operators, defined below Eq. (14), and hence the effective driving rate (15), become time independent. Moreover, under this approximation $\mathcal{P}\mathcal{L}_I^{(2)}(t)\mathcal{P} = 0$, allowing us to largely simplify the Nakajima-Zwanzig equation [27]. Second, we assume that the two-time correlation functions of the bath operators appearing in the interaction Liouvillian (19) decay on a much faster timescale than any characteristic timescale of the system Liouvillian $\mathcal{L}_S^{(2)}(t)$.[1] This assumption is valid provided that $\kappa_{ti} \gg \gamma_n, |\Omega_n'|$ and it allows us to undertake the Markov approximation, namely, to substitute

$$\hat{\rho}_{\rm tot}^{(2)}(\tau) = \hat{\rho}_{B,s}^{(2)}(\tau) \otimes \hat{\rho}_S^{(2)}(\tau) \approx \hat{\rho}_{B,s}^{(2)}(\tau) \otimes \hat{\rho}_S^{(2)}(t) \tag{24}$$

in the integrand of Eq. (22) and take the upper integration limit to infinity [27].

Within the Born-Markov approximation we obtain the master equation for the system dynamics,

$$\frac{d}{dt}\hat{\rho}_S^{(2)}(t) = \mathcal{L}_S^{(2)}(t)\big[\hat{\rho}_S^{(2)}(t)\big] - \int_0^\infty d\tau\, {\rm tr}_B \big[\hat{V}^{(2)}(t), \tilde{\mathcal{G}}(t,\tau)\big[\hat{V}^{(2)}(t-\tau), \hat{\rho}_{B,s}^{(2)}(t-\tau) \otimes \hat{\rho}_S^{(2)}(t)\big]\big], \tag{25}$$

where $\tilde{\mathcal{G}}(t,\tau) = \mathcal{T}_+ \exp[\int_{t-\tau}^t d\tau' \mathcal{B}^{(2)}(\tau')]$. Equation (25) is a generalization of the standard Born-Markov master equation. Note that for a closed ($\mathcal{B} = 0$) and undriven [$\hat{\rho}_{B,s}^{(2)}(t)$ time-independent] TLS bath, Eq. (25) reduces to the usual form more commonly used in simpler open quantum systems [27]. The second term in Eq. (25) captures the TLS-induced dissipation and is completely determined by two-time correlation functions of Pauli operators [36],

$${\rm tr}_B\big[\hat{\tilde{\sigma}}_{\pm i}^{(2)}(t)\tilde{\mathcal{G}}(t,\tau)\big\{\hat{\tilde{\sigma}}_{\pm j}^{(2)}(t-\tau)\hat{\rho}_{B,s}^{(2)}(t-\tau)\big\}\big] \propto \delta_{ij}, \tag{26}$$

where δ_{ij} follows from the independent TLS assumption.

Expanding Eq. (25), the final Born-Markov master equation can be written, in the frame rotating at frequency ω_d, as

$$\dot{\hat{\rho}}_S^{(1)} = -i\big[\hat{H}_S', \hat{\rho}_S^{(1)}\big] + \mathcal{S}\big[\hat{\rho}_S^{(1)}\big] + \mathcal{S}_{\rm TLS}\big[\hat{\rho}_S^{(1)}\big]. \tag{27}$$

The term $\hat{H}_S'$ is given by

$$\hat{H}_S' = \hbar\sum_n \{\Delta_n \hat{s}_n^\dagger \hat{s}_n + (\Omega_n' \hat{s}_n + {\rm H.c.})\} + \hbar\sum_{mn}\{\delta_{mn}\hat{s}_m^\dagger \hat{s}_n + (g_{mn}\hat{s}_m\hat{s}_n + {\rm H.c.})\} \tag{28}$$

and it includes the original system Hamiltonian plus additional coherent dynamics induced by the TLS bath. These dynamics include, first, a modified system driving rate given by Eq. (15) in the Born approximation, namely,

$$\Omega_n' = \Omega_n + \sum_i G_{in}\langle\hat{\sigma}_{+i}\rangle_{\rm ss}, \tag{29}$$

where $\langle\hat{\sigma}_{\alpha i}\rangle_{\rm ss} = {\rm tr}_B[\hat{\sigma}_{\alpha i}\hat{\rho}_{B,s}^{(1)}]$; second, a frequency shift of each system mode and interactions of the beam-splitter type between different system modes (δ_{mn}); and third, interactions of the two-mode squeezing type (g_{mn}), given by the rates

$$\delta_{mn} = -\frac{i}{2}(\Gamma_{+-}^{mn} + \Gamma_{-+}^{mn}) + \frac{i}{2}(\Gamma_{+-}^{nm} + \Gamma_{-+}^{nm})^*, \tag{30}$$

$$g_{mn} = -\frac{i}{2}[\Gamma_{++}^{mn} - (\Gamma_{--}^{nm})^*]. \tag{31}$$

The above rates are expressed in terms of the TLS one-sided power spectral densities

$$\Gamma_{\alpha\beta}^{mn} = \sum_i G_{in}^{(\alpha)} G_{im}^{(\beta)} \int_0^\infty d\tau\, \langle\hat{\tilde{\sigma}}_{\alpha i}(\tau)\hat{\tilde{\sigma}}_{\beta i}(0)\rangle_{\rm ss} e^{\beta i\Delta_m\tau}, \tag{32}$$

where $\alpha, \beta = \pm$, $G_{in}^{(+)} = G_{in}$, $G_{in}^{(-)} = G_{in}^*$, and

$$\langle\hat{\tilde{\sigma}}_{\alpha i}(\tau)\hat{\tilde{\sigma}}_{\beta i}(0)\rangle_{\rm ss} = {\rm tr}_B\big[\hat{\tilde{\sigma}}_{\pm i} e^{\mathcal{L}_B^{(1)}\tau}\big\{\hat{\tilde{\sigma}}_{\pm j}\hat{\rho}_{B,s}^{(1)}\big\}\big] \tag{33}$$

are the two-time correlation functions in the bath steady state. As $\hat{\rho}_{B,s}^{(1)}$ is time independent, the correlators (33) do not depend explicitly on time t. The last term in Eq. (27) describes the dissipative dynamics induced by the TLS bath and it takes the most general form possible for quadratic Lindblad dissipators,

$$\mathcal{S}_{\rm TLS}[\hat{\rho}_S] = \sum_{mn}\big\{(\Gamma_{mn}\mathcal{D}_{\hat{s}_m,\hat{s}_n} + {\rm H.c.}) + \gamma_+^{mn}\mathcal{D}_{\hat{s}_m^\dagger,\hat{s}_n}[\hat{\rho}_S] + \gamma_-^{mn}\mathcal{D}_{\hat{s}_m,\hat{s}_n^\dagger}[\hat{\rho}_S]\big\}. \tag{34}$$

The rates in this equation are given by

$$\gamma_\pm^{mn} = \Gamma_{\pm\mp}^{mn} + (\Gamma_{\pm\mp}^{nm})^* \tag{35}$$

and

$$\Gamma_{mn} = \Gamma_{++}^{mn} + (\Gamma_{--}^{nm})^*. \tag{36}$$

The power spectral densities (32), and hence all the rates in the master equation, can be calculated analytically as a function of the parameters N, Ω_{Bi}, ω_{Bi}, ω_d, κ_{1i}, κ_{2i}, ω_n, and T. Using the optical Bloch equations and the quantum regression theorem [36], we compute the integral

$$\int_0^\infty d\tau\, \langle\hat{\tilde{\boldsymbol{\sigma}}}_i(\tau)\hat{\tilde{\sigma}}_{\pm i}(0)\rangle_{\rm ss}\, e^{\pm i\Delta_m\tau} = -(A_i \pm i\Delta_m \mathbb{1}_3)^{-1}\langle\hat{\tilde{\boldsymbol{\sigma}}}_i\hat{\tilde{\sigma}}_{\pm i}\rangle_{\rm ss}, \tag{37}$$

where $\hat{\tilde{\boldsymbol{\sigma}}}_i = (\hat{\tilde{\sigma}}_{+i}, \hat{\tilde{\sigma}}_{-i}, \hat{\tilde{\sigma}}_{zi})^T$, $\langle\hat{\tilde{\boldsymbol{\sigma}}}_i\hat{\tilde{\sigma}}_{\pm i}\rangle_{\rm ss} = {\rm tr}[\hat{\tilde{\boldsymbol{\sigma}}}_i\hat{\tilde{\sigma}}_{\pm i}\hat{\rho}_{B,s}^{(1)}]$, $\mathbb{1}_d$ is the d-dimensional identity matrix, and A_i is a coefficient matrix given by

$$A_i = \begin{pmatrix} i\Delta_{Bi} - \kappa_{ti} & 0 & -i\Omega_{Bi}^*/2 \\ 0 & -i\Delta_{Bi} - \kappa_{ti} & i\Omega_{Bi}/2 \\ -i\Omega_{Bi} & i\Omega_{Bi}^* & -\kappa_{1i}[1 + 2\bar{n}(\omega_{Bi})] \end{pmatrix}. \tag{38}$$

Introducing Eq. (37) in Eq. (32) and using the commutation relations of the Pauli operators, we obtain analytical expressions for the rates $\Gamma_{\alpha\beta}^{mn}$ in terms of the spectral properties of the matrix A_i and of the stationary-state expectation values of the Pauli operators,

$$\langle\hat{\sigma}_{+,i}\rangle_{\rm ss} = \frac{-1}{1 + 2\bar{n}(\omega_{Bi}) + s_i}\frac{\Omega_{Bi}^*}{2(\Delta_{Bi} + i\kappa_{ti})}, \tag{39}$$

$$\langle\hat{\sigma}_{z,i}\rangle_{\rm ss} = \frac{-1}{1 + 2\bar{n}(\omega_{Bi}) + s_i}, \tag{40}$$

[1] It is at this point where the change of variables in Eq. (14) becomes crucial. Indeed, if the bath operators appearing in the interaction Liouvillian had a nonzero expectation value, some of their two-time correlation functions would not decay, preventing us from performing the Markov approximation.

given in terms of the saturation parameter

$$s_i = \frac{\kappa_{ti}}{\kappa_{1i}} \frac{|\Omega_{Bi}|^2}{\kappa_{ti}^2 + \Delta_{Bi}^2}. \tag{41}$$

The master equation (27) is the main result of this work.

We conclude this section with several remarks. First, note that, due to the Born-Markov approximation, the master equation models an environment of lossy TLSs ($\kappa_{ti} \gg |G_{in}|, \gamma_n, |\Omega'_n|$) and it is thus adequate to model baths of near-resonance solid-state impurities which typically have large linewidths [1,9,15,18,20,22]. However, although our initial model is formally identical to the usual cavity quantum electrodynamics, the derived master equation is not appropriate to describe typical quantum optics cavity QED setups where the TLSs (atoms, quantum dots, etc.) are characterized by a very narrow linewidth κ_{ti}. Second, note that within the Born-Markov approximation it is consistent to consider the TLSs to be in their stationary state, defined by Eq. (21), already at the time $t = 0$, i.e., right after the driving is turned on. Indeed, since the timescale at which the TLSs evolve to their stationary state (given by κ_{ti}^{-1}) is much shorter than the timescale of the system dynamics (given by ${\gamma_n}^{-1}$ and $|\Omega'_n|^{-1}$), this relaxation can be considered instantaneous. Third, note that the most unconventional effective dynamics in the master equation originates exclusively from the driving of the TLS bath. In the absence of this driving, i.e., at $\Omega_{Bi} = 0$, one has $\Omega'_n = \Omega_n$ and $\Gamma_{mn} = g_{mn} = 0$ and the master equation recovers the usual form obtained for simpler baths (e.g., undriven bosonic baths), containing only absorption, decay, and particle-conserving interactions. Finally, note that by following the above steps our derivation can be directly extended to include the following additional features: (i) rotating terms (proportional to $\hat{\sigma}_{-i}\hat{s}_n$ and/or $\hat{\sigma}_{zi}\hat{s}_n$) in the interaction Liouvillian (9); (ii) different driving frequencies $\omega_{d,S}$ and $\omega_{d,B}$ for the system and the bath; (iii) arbitrarily strong system driving[2] Ω_n and/or an arbitrary system dissipator $\mathcal{S}$, as long as their associated timescales are consistent with the Markov approximation; and (iv) a bath composed of multilevel systems with dissipators $\mathcal{B}$ of an arbitrary form, as long as the timescales of these dissipators are consistent with the Born and Markov approximations.

III. TLS-INDUCED DYNAMICS: AMPLIFICATION, SQUEEZING, AND SYSTEM INSTABILITIES

In this section we focus on understanding the effective system dynamics induced by the driven TLS bath. In Sec. III A we introduce the particular case of a single bosonic mode coupled to a bath of N identical TLSs. In Sec. III B we characterize the rates appearing in the master equation for this particular case. In Sec. III C we characterize the steady state of the system and the exotic properties arising from the nonthermal bath.

[2]This can be done by transforming to a different frame, this time with respect to a Hamiltonian including the system driving. A more complicated but still analytical master equation can be derived in this case.

TABLE I. Summary of the parameters in the particular case of a single bosonic mode coupled to a bath of N identical TLSs.

Parameter	Definition
ω_d	driving frequency
ω_0	system frequency
Δ_0	system detuning
Ω_0	external driving rate of the system
γ_0	intrinsic decay rate of the system
ω_B	TLS frequency
Δ_B	TLS detuning
Ω_B	external driving rate of the TLS
κ_1	TLS decay rate
κ_2	TLS dephasing rate
κ_t	TLS transverse decay rate
s	TLS saturation parameter
G	system-TLS coupling rate
Ω'_0	TLS-induced effective driving rate of the system
$\gamma_\pm$	TLS-induced system absorption or emission rate
γ	TLS-induced decay rate
g, Γ	TLS-induced system squeezing rates
δ	TLS-induced system frequency shift

A. Particular case: Single mode coupled to a bath of identical TLSs

To illustrate the rich phenomenology induced by the driven TLS bath, hereafter we focus on the particular case of a single bosonic mode, coupled to a bath of N identical TLSs. The bosonic mode is described by creation and annihilation operators $\hat{s}^\dagger$ and $\hat{s}$, respectively. Its free dynamics, given by $\mathcal{L}_S$ in Eq. (2), is characterized by a frequency ω_0, a driving rate Ω_0, and an intrinsic decay rate γ_0. Since the TLSs are identical, all the rates become TLS independent, i.e., $\{\omega_{Bi}, \kappa_{1i}, \kappa_{2i}, \Omega_{Bi}, G_{in}, \Delta_{Bi}, \kappa_{ti}, s_i\} \to \{\omega_B, \kappa_1, \kappa_2, \Omega_B, G, \Delta_B, \kappa_t, s\}$. Similarly, since this particular case consists of a single mode, for simplicity we denote its TLS-induced master-equation rates $\{\delta_{nn}, g_{nn}, \gamma_\pm^{nn}, \Gamma_{nn}\} \to \{\delta, g, \gamma_\pm, \Gamma\}$. Without loss of generality, we assume $\Omega_B \in \mathbb{R}$. All the parameters appearing in this particular case are summarized in Table I. The master equation in this case has the same form as Eq. (27), with a simplified Hamiltonian

$$\hat{H}'_S = \Delta' \hat{s}^\dagger \hat{s} + (\Omega'_0 \hat{s} + \text{H.c.}) + (g\hat{s}^2 + \text{H.c.}) \tag{42}$$

and a dissipator

$$\mathcal{S}_{\text{TLS}}[\hat{\rho}_S] = \gamma_+ \mathcal{D}_{\hat{s}^\dagger,\hat{s}}[\hat{\rho}_S] + \gamma_- \mathcal{D}_{\hat{s},\hat{s}^\dagger}[\hat{\rho}_S] + (\Gamma \mathcal{D}_{\hat{s},\hat{s}}[\hat{\rho}_S] + \text{H.c.}). \tag{43}$$

Here $\Delta' = \Delta_0 + \delta$, with the system detuning $\Delta_0 = \omega_0 - \omega_d$ and $\Omega'_0 = \Omega_0 + NG\langle\hat{\sigma}_{+i}\rangle$.

From the master equation (27) one can obtain a dynamical equation for the expectation value of any system operator $\hat{S}$, namely, $d\langle\hat{S}\rangle/dt = \text{tr}[\hat{S}\dot{\hat{\rho}}_S^{(1)}]$. Since the master equation is quadratic, the expectation values of the first- and second-order momenta $\boldsymbol{v} = [\langle\hat{s}^\dagger\hat{s}\rangle, \langle\hat{s}\rangle, \langle\hat{s}^\dagger\rangle, \langle\hat{s}^2\rangle, \langle(\hat{s}^\dagger)^2\rangle]^T$ obey a closed linear system of differential equations of the form $\dot{\boldsymbol{v}} = A_S\boldsymbol{v} +$

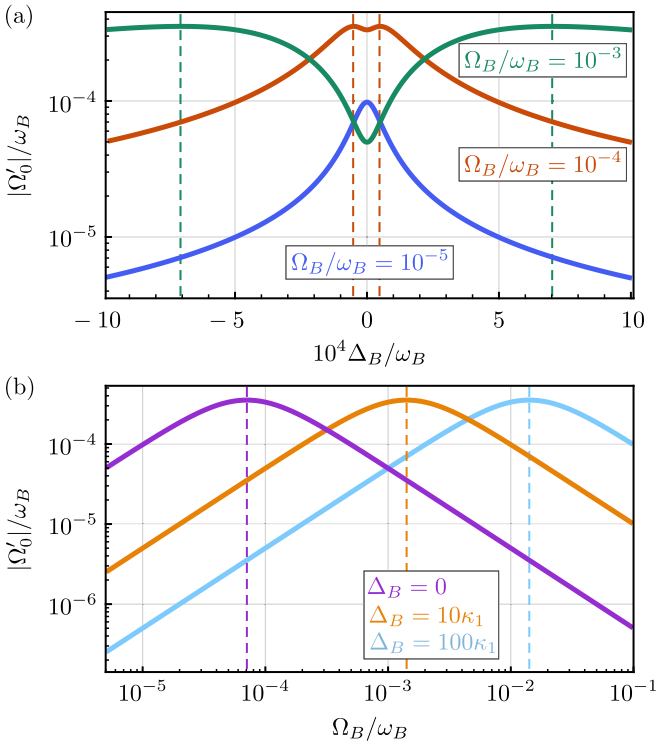

FIG. 2. (a) Dependence of the effective driving rate Ω_0' on the detuning between the TLSs and their driving Δ_B for different values of the TLS driving rate Ω_B. In the red and green curves, vertical dashed lines indicate the optimum detuning $\Delta_{B,\mathrm{opt}} = \pm\sqrt{|\Omega_B|^2/2 - \kappa_t^2}$ (see the text). (b) Dependence of the effective driving rate Ω_0' on TLS driving rate Ω_B at fixed detunings Δ_B. The dashed lines mark the values of the driving rate at which $s = 1$.

$\boldsymbol{a}_S$, with

$$A_S = \begin{pmatrix} -(\gamma_0+\gamma) & i\Omega_0' & -i\Omega_0'^* & 2ig & -2ig^* \\ 0 & \tilde{\Delta}^* & -2ig^* & 0 & 0 \\ 0 & 2ig & \tilde{\Delta} & 0 & 0 \\ -4ig^* & -2i\Omega_0'^* & 0 & 2\tilde{\Delta}^* & 0 \\ 4ig & 0 & 2i\Omega_0' & 0 & 2\tilde{\Delta} \end{pmatrix} \tag{44}$$

and

$$\boldsymbol{a}_S = (\gamma_+, -i\Omega_0'^*, i\Omega_0', -2ig^* - \Gamma^*, 2ig - \Gamma)^T. \tag{45}$$

In the above equations we define $\tilde{\Delta} = i\Delta' - (\gamma_0+\gamma)/2$, where the important parameter $\gamma = \gamma_- - \gamma_+$ is the TLS-induced decay rate of the system. In the following we analyze the rates and the effective dynamics induced by the TLS in this particular scenario.

B. Master-equation rates: Mollow sidebands and amplification

We divide this section into three blocks corresponding to the effective system driving rate Ω_0', the rates associated with particle-non-conserving terms Γ and g, and the decay rate and frequency shift γ and δ, respectively.

TABLE II. Default values chosen for the parameters in all the figures throughout the text. All the rates are expressed in terms of the TLS frequency ω_B.

Parameter	Value
temperature	$T = 0$
system-TLS coupling rate	$G = 10^{-8}\omega_B$
number of the TLS	$N = 10^5$
TLS decay rate	$\kappa_1 = 10^{-4}\omega_B$
TLS dephasing rate	$\kappa_2 = 0$
system decay rate	$\gamma_0 = 10^{-7}\omega_B$

1. *Effective driving rate* Ω_0'

We first consider the effective driving rate Ω_0'. For simplicity, we assume the system is not independently driven, i.e., $\Omega_0 = 0$, so that $\Omega_0' = NG\langle\hat{\sigma}_{+i}\rangle$. This rate originates from the expectation value of the TLS operators. Its effect on the system is analogous to the *coherent* electromagnetic scattering of a driven TLS, namely, to the coherent part of the resonance fluorescence spectrum [34,35]. In the context of resonance fluorescence, the coherent scattering results from the emission of light by the classical component of the TLS dipole moment. Indeed, the square modulus of the effective driving rate reads

$$|\Omega_0'|^2 = (N|G|)^2 \frac{\kappa_1}{4\kappa_t} \frac{s}{(1+s)^2}, \tag{46}$$

where s is the saturation parameter (41) characterizing the regimes of strong ($s \gg 1$) and weak ($s \ll 1$) TLS driving. Equation (46) has an identical dependence on the saturation parameter as the coherently scattered power in resonance fluorescence [34,35].

The effective driving rate Ω_0' is shown in Fig. 2(a) as a function of detuning between the TLSs and their driving Δ_B and for different values of the TLS driving rate Ω_B. The remaining parameters, chosen as in Table II, are consistent with our approximations and with typical values in microwave and magnonics platforms. At weak driving $\Omega_B \ll \kappa_t$ (blue curve) the saturation parameter is always low $s \ll 1$ [see Eq. (41)] and the effective driving rate has a single peak at $\Delta_B = 0$, as $|\Omega_0'| \sim \sqrt{s}$. As the driving rate reaches values comparable to the TLS linewidth $\Omega_B \sim \kappa_t$, the saturation parameter can become $s \gtrsim 1$. In this regime the effective driving rate acquires a double-peaked structure as shown by the red and green curves in Fig. 2(a). This is a characteristic indication of the energy levels of the TLS becoming dressed by the strong driving, with eigenenergies $\pm\hbar\sqrt{\Delta_B^2 + |\Omega_B|^2}/2$.[3] As a consequence of this shift in the TLS bare energies, the driving is not resonant anymore at $\Delta_B = 0$ and the conditions for maximum scattering shift to detunings $\Delta_{B,\mathrm{opt}}^2 = |\Omega_B|^2/2 - \kappa_t^2 \neq 0$, marked by vertical dashed lines in Fig. 2(a). The above argument is confirmed by Fig. 2(b), where we show the effective driving rate at fixed detuning Δ_B as a function of driving rate Ω_B. At weak driving it grows linearly, whereas at strong driving it linearly decays, $|\Omega_0'| \propto 1/\sqrt{s} \propto 1/\Omega_B$, as the fixed driving

[3]This can be readily checked by diagonalizing the TLS Hamiltonian (6) in the frame rotating at the driving frequency.

frequency becomes increasingly off-resonance with respect to the energy gap between the dressed TLS states. The maximum of Ω_0' is attained at $s = 1$ [see Eq. (46)], marked by vertical dashed lines in Fig. 2(b). As the detuning Δ_B increases, the condition $s = 1$ is attained at larger driving rates Ω_B, and thus the curves in Fig. 2(b) shift forward horizontally.

2. *Squeezing rates* Γ *and* g

All the remaining rates in Eqs. (42) and (43), namely, γ, δ, Γ, and g, originate from the fluctuations of the TLS bath, i.e., from the Fourier transform of the two-time correlation functions $\langle\hat{\tilde{\sigma}}_{\alpha i}(t+\tau)\hat{\tilde{\sigma}}_{\beta i}(t)\rangle$ with $\alpha, \beta = \pm$, evaluated at the system frequency Δ_0 [see Eq. (32)]. These rates and their associated effective dynamics thus show some properties similar to the *incoherent* scattering spectrum of resonance fluorescence, as we will see below. Here we focus on the two rates Γ and g which arise from correlators $\langle\hat{\tilde{\sigma}}_{\alpha i}(t+\tau)\hat{\tilde{\sigma}}_{\alpha i}(t)\rangle$. They represent a contribution to the system effective dynamics exclusively induced by the driving of the bath, as they vanish at $\Omega_B = 0$. Both Γ and g appear in excitation-nonconserving terms in the master equation and can induce squeezing and instabilities on the system, as we will see below. As evidenced by Eqs. (44) and (45), the dissipator associated with Γ only affects the steady state of the system while leaving any dynamical rate unchanged.

In the following we focus on the case of resonantly driven TLSs, namely, $\omega_B = \omega_d$ ($\Delta_B = 0$). The rates Γ and g are displayed in Figs. 3(a) and 4(a), respectively, as a function of the system detuning Δ_0 for three values of the driving rate Ω_B and the parameters in Table II. In this regime, the analytical expressions can be derived,

$$\begin{pmatrix} g \\ \Gamma \end{pmatrix} = \frac{NG^2}{2\kappa_1}\frac{-s}{(1+s)^2 f(s,\Delta_0/\kappa_1)} \times \begin{pmatrix} i(i\Delta_0/\kappa_1 - 1)(1+s) \\ s^2 + 2s + 4(i\Delta_0/\kappa_1 - 1)^2 \end{pmatrix}, \tag{47}$$

with $f(s,d) = [s + 2(id-1)(id-\frac{1}{2})](id-\frac{1}{2})$. At low saturation $s \ll 1$ [blue curves in Figs. 3(a) and 4(a)] the rates have a Lorentzian profile, as $\Gamma, g \sim s$. At high saturation $s \gg 1$ (green curves) two additional side peaks emerge. This is a manifestation of the large dressing of the TLS energy levels by the strong coherent driving, analogous to the AC Stark shift in quantum optics that produces the Mollow triplet [37]. In general, the Mollow triplet appears when the energy gap between the dressed states of the TLS becomes larger than their linewidth. For the parameters of Figs. 3(a) and 4(a), this condition reads $|\Omega_B| > \kappa_t/2$ and the side emission peaks arise at frequencies $\sqrt{|\Omega_B|^2 - (\kappa_t/2)^2}$, indicated by the vertical dashed lines.

The dependence of the rates Γ and g on the TLS driving rate Ω_B is shown in Figs. 3(b) and 4(b), respectively, for two values of the system detuning Δ_0. While the coherent rate g vanishes in the strong driving limit, where $g \sim s^{-1}$, the dissipative rate Γ saturates to a value given by

$$\lim_{s\to\infty}\Gamma = \frac{NG^2}{2(\kappa_t - i\Delta_0)}. \tag{48}$$

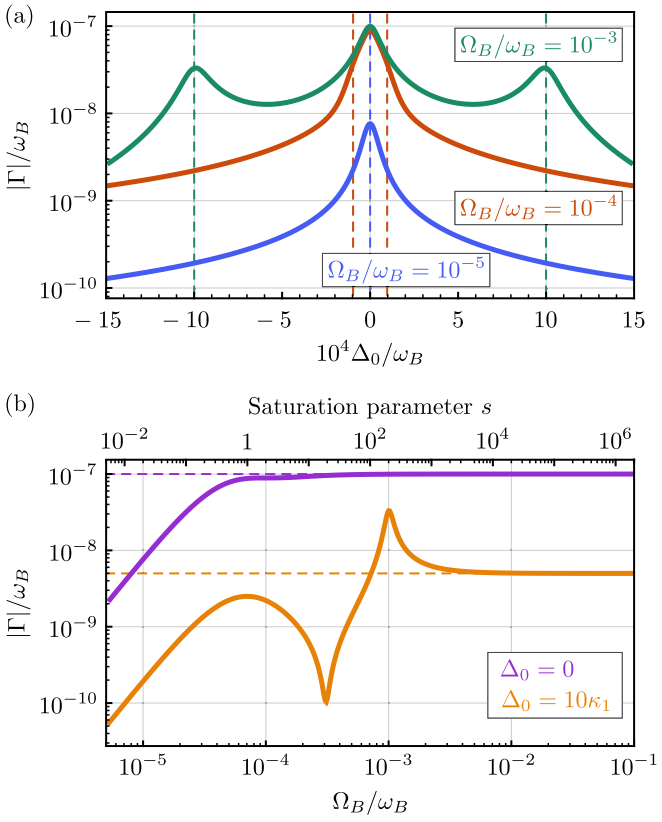

FIG. 3. (a) Dependence of the rate Γ on the system detuning Δ_0 for $\Delta_B = 0$, different TLS driving rates Ω_B, and the parameters in Table II. The dashed lines denote the frequencies of the Mollow sidebands (see the text). (b) Dependence of the rate Γ on TLS driving rate Ω_B for different system detunings Δ_0 and the same parameters as in (a). The horizontal dashed lines denote the strong-driving limit (48).

Note that Eq. (48) is valid for any finite TLS detuning Δ_B. Both the saturation of Γ and the appearance of a Mollow triplet are identifying characteristics of incoherent resonance fluorescence spectra [34,35]. We can thus understand the rates g and Γ as stemming from the TLS incoherently pumping energy from the driving into the system or vice versa. Note that, since in our case the system does not show a continuous energy spectrum but a single resonance at frequency ω_0 (in the rotating frame, Δ_0), it resembles more closely the more involved situation of TLS resonance fluorescence inside an optical cavity [38–47]. Specifically, the system acts as a "frequency filter," probing the incoherent scattering spectrum within a narrow frequency window [38]. This is evidenced by Figs. 3(b) and 4(b) where for $\Delta_0 = 0$ (purple curves) only the energy scattered at the TLS natural frequency (i.e., only the central peak of the Mollow triplet) contributes to the rates, which thus monotonically depend on Ω_B. Conversely, when the system is detuned $\Delta_0 \neq 0$ (orange curves), the rates $|g|$ and $|\Gamma|$ reach a maximum at the value Ω_B at which the Mollow side peak and the system become resonant [compare with Figs. 3(a) and 4(a)].

3. *Decay rate* γ *and frequency shift* δ

We finally focus on the decay rate γ and the frequency shift δ. Since these result from the TLS correlators $\langle\hat{\tilde{\sigma}}_{\pm i}(t+$

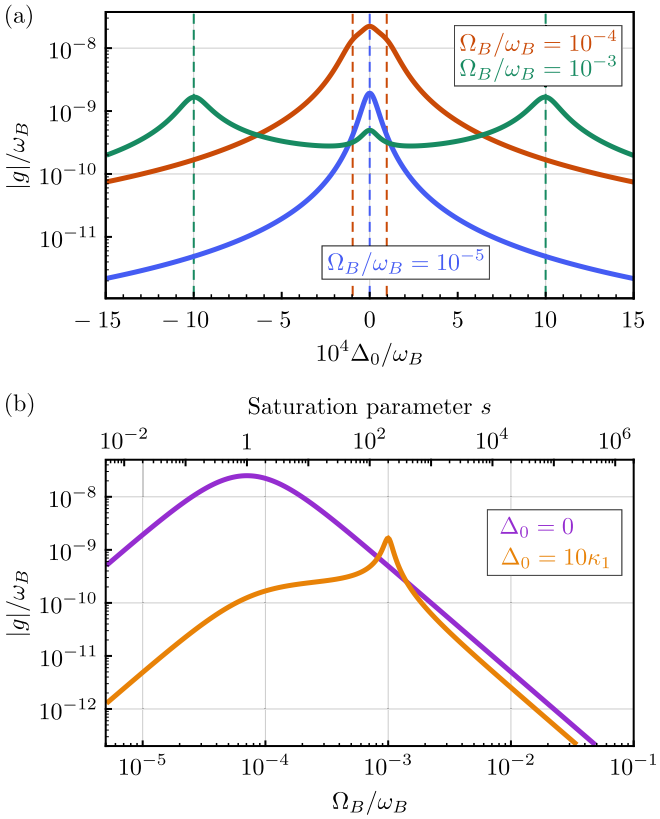

FIG. 4. (a) Dependence of the rate g on the system detuning Δ_0 for $\Delta_B = 0$, different TLS driving rates Ω_B, and the parameters in Table II. The dashed lines denote the frequencies of the Mollow sidebands (see the text). (b) Dependence of the rate g on TLS driving rate Ω_B for different system detunings Δ_0 and the same parameters as in (a).

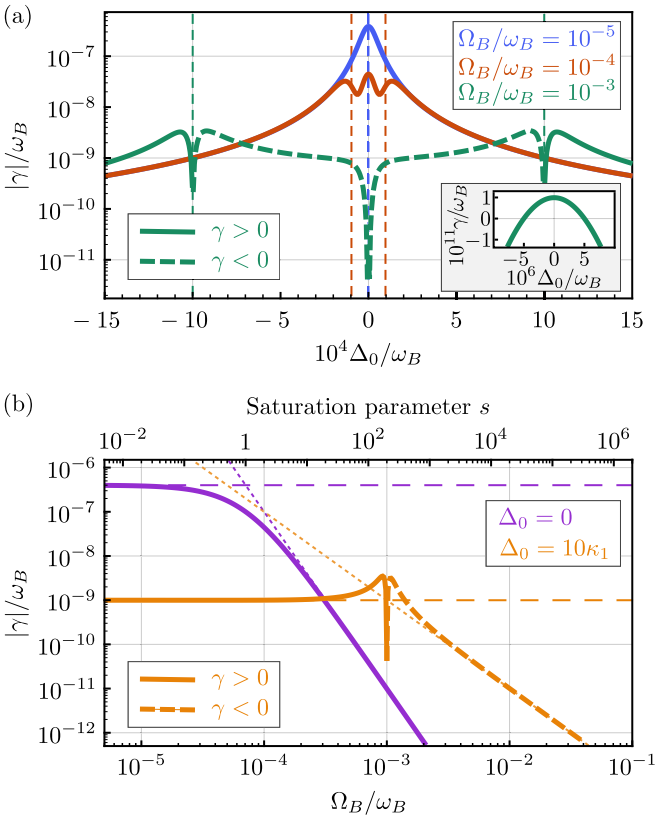

FIG. 5. (a) Dependence of the decay rate γ on the system detuning Δ_0 for $\Delta_B = 0$, different TLS driving rates Ω_B, and the parameters in Table II. The dashed lines denote the frequencies of the Mollow sidebands (see the text). The inset shows a close-up of the green curve at small system detunings $|\Delta_0| \lesssim \kappa_t$. (b) Dependence of the decay rate γ on the TLS driving rate Ω_B for different system detunings Δ_0 and the same parameters as in (a). The horizontal dashed lines indicate the no-driving limit (49), whereas the dotted lines indicate the high-driving limits (50).

$\tau)\hat{\tilde{\sigma}}_{\mp i}(t)\rangle$, they do not vanish in the low TLS driving limit, where

$$\lim_{s\to 0}\begin{pmatrix}\gamma\\ \delta\end{pmatrix} = \frac{N|G|^2}{\kappa_t^2 + (\omega_0-\omega_B)^2} \times \tanh\left[\frac{\hbar\omega_B}{2k_BT}\right]\begin{pmatrix}2\kappa_t\\ \omega_0-\omega_B\end{pmatrix}. \tag{49}$$

The above expression for γ, which is also valid for $\Delta_B \neq 0$, coincides with the predictions of the standard tunneling model for a bath of undriven TLSs [23]. In the opposite limit of strongly driven TLSs the decay rate and the frequency shift vanish, $\lim_{s\to\infty}\gamma = \lim_{s\to\infty}\delta = 0$, as the TLSs become saturated and thus induce neither absorption nor decay. The suppression of γ for a saturated TLS bath has been demonstrated in acoustic and magnonic setups [15,18,48]. Both rates γ and δ capture two different physical phenomena affecting the system. On the one hand, similarly to the rates g and Γ analyzed in the preceding section, the rates γ and δ represent a part of the incoherent scattering of the TLS driving into the system, as they originate from the fluctuations of the TLS operators. On the other hand, they describe the contact, mediated by the TLS, between the system and the thermal reservoir inducing the TLS dissipation, as evidenced by the nonzero value of Eq. (49). Because of the competition between these two processes, the rates γ and δ display a particularly rich phenomenology.

Let us focus on the decay rate γ. This rate is shown in Fig. 5(a) as a function of the system detuning Δ_0 for three values of the driving rate Ω_B and the parameters in Table II. At weak driving $s \ll 1$ (blue curve) it displays the usual Lorentzian profile given by Eq. (49), whereas at higher driving (red and green curves) different regimes appear depending on the detuning Δ_0. In the strongly driven case $s \gg 1$ the rate γ can, remarkably, become negative, indicating that, instead of damping, the TLS bath induces amplification of the system dynamics.[4] As evidenced by Fig. 5(a) and the inset, amplification occurs at system-TLS detunings fulfilling $\kappa_t \lesssim |\Delta_0| \leqslant$

[4]Note that for $\gamma < 0$ the system can still be damped if its additional damping mechanisms dominate, i.e., if $\gamma_0 + \gamma > 0$.

Ω_B. This behavior is captured analytically through the limits

$$\lim_{s\to\infty}\gamma = N|G|^2\kappa_1 \times \begin{cases} \Delta_0^{-2} & \text{for } \Delta_0 \gg \Omega_B \gg \kappa_t \\ -\Omega_B^{-2} & \text{for } \Omega_B \gg \Delta_0 \gg \kappa_t \\ 2\kappa_1\kappa_t\Omega_B^{-4}\coth\left[\frac{\hbar\omega_B}{2k_BT}\right] & \text{for } \Omega_B \gg \kappa_t \gg \Delta_0, \end{cases} \quad (50)$$

denoted by the dotted lines in Fig. 5(b), where we show the dependence of γ on the TLS driving rate Ω_B (solid curves). The behavior of γ and especially the amplification $\gamma < 0$ is a consequence of the nonthermal state of the TLS bath [45]. Indeed, the TLS bath is simultaneously coupled to a thermal reservoir at temperature T, which tends to drive it into a thermal state and to an external driving which, in the limit $s \gg 1$, tends to drive it into a fully unpolarized state $\hat{\rho}_B = \mathbb{1}_{2N}/2$, effectively acting as an infinite-temperature thermal reservoir. For some parameter combinations and in the regime of strong driving $\Omega_B \gg \kappa_t$, this results in continuous pumping of energy into the system. The behavior of the resulting amplification, captured by Fig. 5, is consistent with the well-known amplification of resonance fluorescence for TLSs inside an electromagnetic cavity [38,44–46,49]. In the platforms we aim at describing in this work, namely, baths of solid-state TLS impurities affecting, e.g., microwave, acoustic, or magnonic resonators, our model predicts a similar amplification.

We can heuristically understand the qualitative behavior of γ through the simpler model of a system with frequency Δ_0 coupled to a single lossy TLS via Jaynes-Cummings interaction $\sim g_0(\hat{s}\hat{\sigma}_+ + \text{H.c.})$, described by an arbitrary coupling rate g_0. At resonant ($\Delta_B = 0$) and strong ($s \gg 1$) driving the TLS is fully dressed, i.e., it is described by the dressed eigenstates $|\pm\rangle = (|e\rangle \pm |g\rangle)/\sqrt{2}$, where $|g\rangle$ ($|e\rangle$) denotes the TLS ground (excited) state. The energies of the dressed eigenstates are $\pm\Omega_B/2$. We can now write the system-TLS interaction in terms of the dressed transition matrices $\hat{\sigma}'_{\alpha\beta} = |\alpha\rangle\langle\beta|$ ($\alpha, \beta = \pm$) and retain only the slowly oscillating terms under a rotating-wave approximation. The validity of the rotating-wave approximation and the form of the resulting interaction Hamiltonian depend on Δ_0. Specifically, for $\kappa_t \ll |\Delta_0| \sim \Omega_B$ and assuming $|\Delta_0 - \Omega_B|, g_0 \ll |\Delta_0| + \Omega_B$, the Hamiltonian reads $\sim(\hat{s}\hat{\sigma}'_{+-} + \text{H.c.})$, while for $|\Delta_0| \lesssim \kappa_t \ll \Omega_B$ and assuming $g_0 \ll \Omega_B$ it reads $\sim(\hat{s} + \hat{s}^\dagger)(\hat{\sigma}'_{++} - \hat{\sigma}'_{--})$. Let us examine in these cases the system emission and absorption rates γ_- and γ_+, respectively, and the total decay rate $\gamma = \gamma_- - \gamma_+$. We further simplify our toy model by assuming that only energy-conserving first-order processes contribute to these rates. First, in the case $\kappa_t \ll |\Delta_0|$, system emission and absorption involve a single transition between the two TLS dressed states plus, if $\Delta_0 \neq \Omega_B$, an additional energy exchange between the TLS and its own thermal reservoir in order to conserve energy. By examination of the respective processes one can infer that $\gamma_- \to \gamma_+$ if $\Delta_0 = \Omega_B$ and $\gamma_\alpha \propto \bar{n}(|\Omega_B - |\Delta_0||) + \delta_{\alpha,\text{sgn}[\Omega_B - |\Delta_0|]}$ if $\Delta_0 \neq \Omega_B$, with $\delta_{\alpha,\beta}$ the Kronecker delta. This simple model thus qualitatively captures the positive (negative) values of γ for positive (negative) values of $\Omega_B - |\Delta_0|$ [see Fig. 5(a)]. In the second case, namely, the regime $|\Delta_0| \lesssim \kappa_t$, the interaction contains only the matrices $\hat{\sigma}'_{\alpha\alpha}$, and hence absorption and emission processes involve no transition between the dressed TLS states. The system thus effectively exchanges energy directly with the thermal reservoir of the TLS, which, being in thermal equilibrium, necessarily results in $\gamma > 0$. Our heuristic argument thus also captures the behavior of γ at small Δ_0 [inset of Fig. 5(a)].

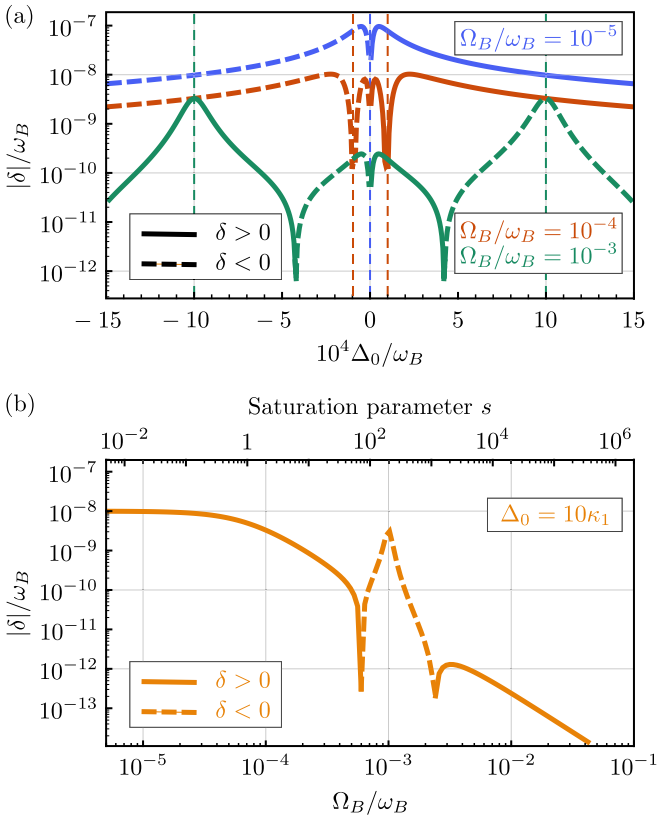

FIG. 6. (a) Dependence of the frequency shift δ on the system detuning Δ_0 for $\Delta_B = 0$, different TLS driving rates Ω_B, and the parameters in Table II. The dashed lines denote the frequencies of the Mollow sidebands (see the text). (b) Dependence of the frequency shift δ on the TLS driving rate Ω_B for a system detuning $\Delta_0 = 10\kappa_t$ and the same parameters as in (a).

For completeness we display in Fig. 6(a) the frequency shift δ as a function of the system detuning Δ_0 for the same parameters as in Fig. 5. In the weak driving regime (blue curve) the frequency shift displays the form given by Eq. (50). This is the usual profile obtained when computing the electromagnetic response function of two-level systems, e.g., in atomic optics [34]. At stronger driving rates, peaks emerge at the Mollow sideband frequencies, confirming the incoherent scattering contribution. The dependence of the frequency shift δ on the TLS driving rate Ω_B is shown in Fig. 6(b) for the same parameters as in Fig. 5. For $\Delta_0 = 0$ the frequency shift is exactly zero.

C. Steady-state properties: Squeezing and dynamical instabilities

In this section we focus on the impact of the TLS bath on the system, specifically on its steady state. We consider a relevant particular case, namely, an undriven system

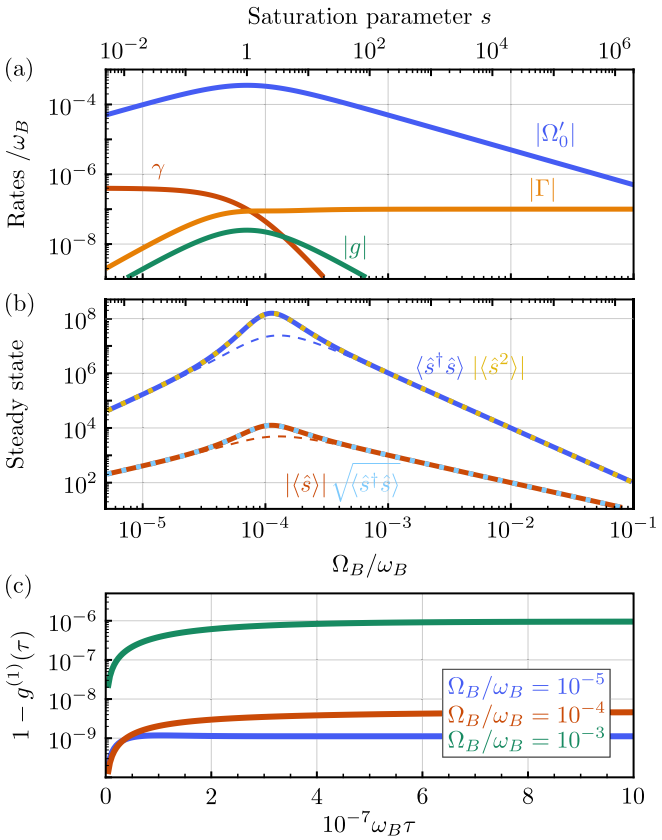

FIG. 7. (a) Master-equation rates as a function of the TLS driving rate Ω_B for the resonant case $\omega_0 = \omega_B = \omega_d$. The frequency shift in this case is $\delta = 0$. (b) Steady-state value of the system operators (solid and dotted curves) as a function of the TLS driving rate Ω_B. The dashed curves show the approximate solution given by Eq. (51). (c) First-order coherence function $g^{(1)}(\tau)$ [Eq. (52)] for three different TLS driving rates Ω_B. In all panels we take the parameter values of Table II.

($\Omega_0 = 0$) in resonance both with the TLSs and with their driving, i.e., $\omega_0 = \omega_B = \omega_d$. The master-equation rates in this case are shown in Fig. 7(a) for the parameters of Table II. For these parameters the bath does not induce amplification, as $\gamma + \gamma_0 > 0\,\forall\, s$. Among the three terms resulting from TLS correlators, namely, γ, g, and Γ, the decay rate γ dominates at low saturation $s \lesssim 1$, whereas the rate Γ dominates at high saturation $s \gtrsim 1$. Any exotic effect ascribed to the nonthermal state of the TLS will thus appear in the regime of unconventional dissipation $s \gtrsim 1$. The squeezing rate g is typically much smaller than the dissipation rates γ and Γ. Regardless of the predominant dissipation, as shown by Fig. 7(a), the effective dynamics is dominated by the coherent driving rate Ω_0'. The strong impact of this effective driving has been experimentally observed in high-Q microwave cavities [48].

Since the master equation (27) is quadratic, the steady state is Gaussian [50]. It is completely determined by the first- and second-order momenta $\boldsymbol{v}_{\rm ss} = (\langle\hat{s}^\dagger\hat{s}\rangle, \langle\hat{s}\rangle, \langle\hat{s}^\dagger\rangle, \langle\hat{s}^2\rangle, \langle(\hat{s}^\dagger)^2\rangle)^T_{\rm ss} = -A_S^{-1}\boldsymbol{a}_S$, where the matrix A_S and the vector $\boldsymbol{a}_S$ are given by Eqs. (44) and (45), respectively. In Fig. 7(b) we show the steady-state values $|\langle\hat{s}\rangle_{\rm ss}|$ (solid red curve), $\langle\hat{s}^\dagger\hat{s}\rangle_{\rm ss}$ (solid blue curve), and $|\langle\hat{s}^2\rangle_{\rm ss}|$ (dotted yellow curve) for the same parameters as in Fig. 7(a). The thin dashed red and blue curves in the figure correspond to the limit $g \to 0$, where the steady state is analytically approximated by

$$\langle\hat{s}^\dagger\hat{s}\rangle_{\rm ss} \approx \frac{\gamma_+}{\gamma} + \frac{4|\Omega_0'|^2}{\gamma^2}, \quad \langle\hat{s}^\dagger\rangle_{\rm ss} \approx \frac{2i\Omega_0'}{\gamma}. \tag{51}$$

As shown by Fig. 7(b) the expressions (51) are very similar to the exact solution except in the vicinity of $s = 1$. Thus, neglecting the small rate g is a good approximation to obtain the values of $|\langle\hat{s}\rangle_{\rm ss}|$ and $\langle\hat{s}^\dagger\hat{s}\rangle_{\rm ss}$. Since the effective coherent driving, given by the rate Ω_0', is the dominant effect in the master equation, the steady state of the system is close to a coherent state, i.e., $\langle\hat{s}^\dagger\hat{s}\rangle_{\rm ss} \approx |\langle\hat{s}\rangle_{\rm ss}|^2 \approx |\langle\hat{s}^2\rangle_{\rm ss}|$, as indicated by Fig. 7(b). This is confirmed by Fig. 7(c), where we display the first-order coherence of the steady state, defined as [34,36]

$$g^{(1)}(\tau) = \frac{\langle\hat{s}^\dagger(0)\hat{s}(\tau)\rangle_{\rm ss}}{\langle\hat{s}^\dagger\hat{s}\rangle_{\rm ss}}, \tag{52}$$

for different values of the TLS driving rates corresponding to $s \ll 1$ (blue curve), $s \sim 1$ (red curve), and $s \gg 1$ (green curve). Although due to the dissipative dynamics the first-order coherence deviates from 1, it remains close to this value at all times, confirming the quasicoherent nature of the steady state.

Despite being close to a coherent state, the steady state is far from the conventional steady state of a driven lossy harmonic oscillator. To show this, we first focus on the conditions for the existence of a steady state. The master equation (27) has a steady state if and only if the system of equations governing $\boldsymbol{v}_{\rm ss}$ is linearly stable [50], i.e., if $\max[{\rm Re}(\lambda_j)] \leqslant 0$, with λ_j ($j = 1, \ldots, 5$) the eigenvalues of A_S. In the resonant case under study, $\omega_0 = \omega_B = \omega_d$, the system is linearly stable if

$$\gamma_0 + \gamma \geqslant 4|g|. \tag{53}$$

In Fig. 8(a) we show a stability diagram for the system as a function of the bare system linewidth γ_0 and the TLS driving rate Ω_B. For a saturated bath ($s \gg 1$) or for a bath in thermal equilibrium ($s \ll 1$) the system is always stable as $g \to 0$ and γ either vanishes or is always positive. Stability is also guaranteed at large enough γ_0, where the decay of the system to its additional bath (assumed in equilibrium; see Sec. II) dominates over the TLS-induced dissipation. However, at intermediate values of s the system can become dynamically unstable. Remarkably, the dynamical instability can originate either from a strong amplification ($\gamma < 0$; see the preceding section) or, as is the case in Fig. 8(a), from a large enough value of the squeezing rate g [51]. Note that since the small rate g plays a relevant role in determining stability, the approximations at $g \to 0$ [Eq. (51)] become inaccurate when the system is near the instability regime. The dynamics in this critical, nearly unstable regime is very sensitive to the value of g, a property that could be used to accurately measure this rate.

The second unconventional feature of the system's steady state is the presence of squeezing. We analyze squeezing in the stable regime, where the steady state exists and it is Gaussian,

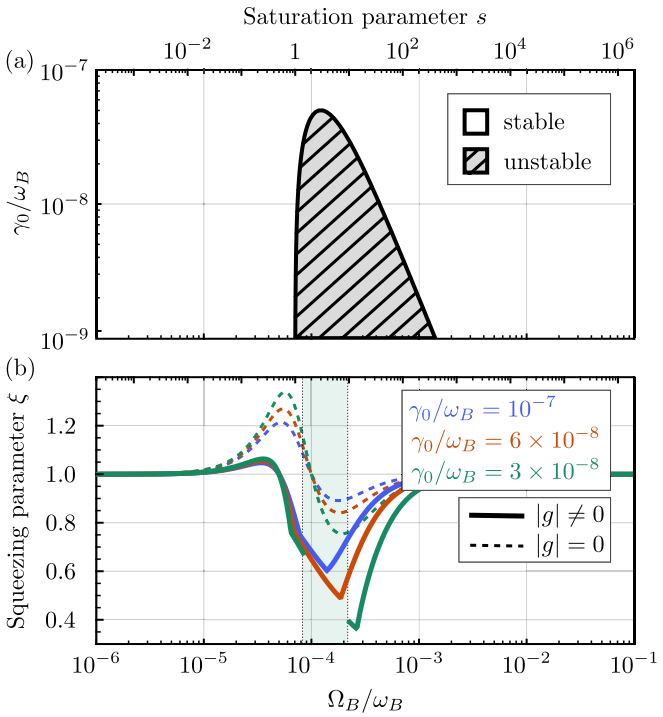

FIG. 8. (a) System stability diagram as a function of the TLS driving rate Ω_B and the system decay rate γ_0, obtained by considering the stability criterion (53). (b) Dependence of the squeezing parameter ξ on the TLS driving rate Ω_B for different system decay rates γ_0. Solid curves show the results for the full model and dashed curves the solution for $g \to 0$. For the smallest decay rate depicted here (green curve), the squeezing parameter ξ is not well defined in the unstable region denoted by the shaded green area.

by computing its covariance matrix [52]

$$\sigma = \begin{pmatrix} V_x & C_{xp} \\ C_{xp} & V_p \end{pmatrix}, \tag{54}$$

where $V_x = \langle (\hat{x} - \langle \hat{x} \rangle)^2 \rangle$, $V_p = \langle (\hat{p} - \langle \hat{p} \rangle)^2 \rangle$, and $C_{xp} = \{\hat{x} - \langle \hat{x} \rangle, \hat{p} - \langle \hat{p} \rangle\}/2$, with $\hat{x} = (\hat{s} + \hat{s}^\dagger)/\sqrt{2}$ and $\hat{p} = i(\hat{s}^\dagger - \hat{s})/\sqrt{2}$ being the quadrature operators. The system squeezing can be quantified via the squeezing parameter $\xi = 1/\sqrt{2 \min_k(\lambda_k)}$, where $\lambda_k \in \mathbb{R}^+$ are the eigenvalues of Eq. (54) [52]. The state is squeezed when $\xi > 1$, and larger values of ξ correspond to larger squeezing. In Fig. 8(b) we plot the squeezing parameter ξ (solid curves) as a function of the TLS driving rate for different values of the system decay rates γ_0. The shaded green area marks the instability window for $\gamma_0/\omega_B = 3 \times 10^{-8}$ [compare with Fig. 8(a)]. According to Fig. 8(b), the steady state of the system is squeezed for a range of saturation parameters around $s \approx 0.1$. Larger squeezing is attained at low values of γ_0, where the TLS-induced dissipation dominates over the system intrinsic dissipation. The steady-state squeezing has both coherent and dissipative contributions, coming from the rates g and Γ, respectively. This is proven by the dashed curves in Fig. 8(b), which depict the squeezing parameter obtained under the substitution $g \to 0$. Remarkably, the squeezing is reduced in the presence of both mechanisms, i.e., when $g, \Gamma \neq 0$, as the corresponding terms in the master equation induce squeezing in mutually orthogonal directions in phase space. The comparison between the dashed and solid curves in Fig. 8(b) also shows that, although approximating $g \to 0$ remains a useful approximation for some steady-state properties such as the occupation number $\langle \hat{s}^\dagger \hat{s} \rangle_{\rm ss}$, it critically fails to capture others such as stability and squeezing. We finally note that the steady-state squeezing is in principle experimentally observable in magnonics or acoustic platforms, where the regime $s \approx 1$ can be achieved [14,15,18,53].

IV. CONCLUSION

We have developed a theoretical model describing the effective dynamics of a system in the presence of a coherently driven two-level-system bath. This has been done by explicitly tracing out the bath degrees of freedom to obtain a Born-Markov master equation. In the limit of weak TLS driving, our results recover the expression given by the standard tunneling model for undriven TLS baths. In the limit of strong TLS driving, our model predicts a vanishing linewidth due to saturated TLSs, as observed in experiments. In the intermediate driving regime exotic dynamics arises as the state of the TLS bath is maximally out of thermal equilibrium. Specifically, the TLS can induce linear instability of the system, either through negative linewidth (amplification) or through single-mode squeezing. Moreover, in the linearly stable regime the steady state of the system is squeezed. From a theoretical point of view, an interesting outlook consists of characterizing the non-Markovian effects arising for nonmonochromatic TLS driving [31–33] or for more strongly coupled and/or less lossy TLS baths.

To conclude, our model provides a theoretical tool for studying, from the quantum optics perspective, the complex TLS baths affecting most quantum technological platforms. It proves that external driving of these baths can be used as a tool not only to minimize dissipation, e.g., by saturating the TLS, but also to probe the TLS bath and acquire deeper information about its properties.

ACKNOWLEDGMENTS

We thank A. Gonzalez-Tudela and Y. Nakamura for helpful discussions. C.G.-B. acknowledges support from the European Union (PWAQUTEC, H2020-MSCA-IF-2017, Grant No. 796725).

[1] A. L. Burin, S. Matityahu, and M. Schechter, Low-temperature $1/f$ noise in microwave dielectric constant of amorphous dielectrics in Josephson qubits, Phys. Rev. B **92**, 174201 (2015).

[2] P. V. Klimov, J. Kelly, Z. Chen, M. Neeley, A. Megrant, B. Burkett, R. Barends, K. Arya, B. Chiaro, Y. Chen, A. Dunsworth, A. Fowler, B. Foxen, C. Gidney, M. Giustina, R. Graff, T. Huang, E. Jeffrey, E. Lucero, J. Y. Mutus *et al.*,

Fluctuations of Energy-Relaxation Times in Superconducting Qubits, Phys. Rev. Lett. **121**, 090502 (2018).

[3] J. Goetz, F. Deppe, P. Eder, M. Fischer, M. Müting, J. P. Martínez, S. Pogorzalek, F. Wulschner, E. Xie, K. G. Fedorov, A. Marx, and R. Gross, Second-order decoherence mechanisms of a transmon qubit probed with thermal microwave states, Quantum Sci. Technol. **2**, 025002 (2017).

[4] S. Schlör, J. Lisenfeld, C. Müller, A. Bilmes, A. Schneider, D. P. Pappas, A. V. Ustinov, and M. Weides, Correlating Decoherence in Transmon Qubits: Low Frequency Noise by Single Fluctuators, Phys. Rev. Lett. **123**, 190502 (2019).

[5] J. J. Burnett, A. Bengtsson, M. Scigliuzzo, D. Niepce, M. Kudra, P. Delsing, and J. Bylander, Decoherence benchmarking of superconducting qubits, npj Quantum Inf. **5**, 54 (2019).

[6] J. Burnett, L. Faoro, I. Wisby, V. L. Gurtovoi, A. V. Chernykh, G. M. Mikhailov, V. A. Tulin, R. Shaikhaidarov, V. Antonov, P. J. Meeson, A. Y. Tzalenchuk, and T. Lindström, Evidence for interacting two-level systems from the $1/f$ noise of a superconducting resonator, Nat. Commun. **5**, 4119 (2014).

[7] S. E. de Graaf, L. Faoro, J. Burnett, A. A. Adamyan, A. Y. Tzalenchuk, S. E. Kubatkin, T. Lindström, and A. V. Danilov, Suppression of low-frequency charge noise in superconducting resonators by surface spin desorption, Nat. Commun. **9**, 1143 (2018).

[8] C. Müller, J. H. Cole, and J. Lisenfeld, Towards understanding two-level-systems in amorphous solids: Insights from quantum circuits, Rep. Prog. Phys. **82**, 124501 (2019).

[9] J. O. Tenorio-Pearl, E. D. Herbschleb, S. Fleming, C. Creatore, S. Oda, W. I. Milne, and A. W. Chin, Observation and coherent control of interface-induced electronic resonances in a field-effect transistor, Nat. Mater. **16**, 208 (2017).

[10] A. Pourkabirian, M. V. Gustafsson, G. Johansson, J. Clarke, and P. Delsing, Nonequilibrium Probing of Two-Level Charge Fluctuators Using the Step Response of a Single-Electron Transistor, Phys. Rev. Lett. **113**, 256801 (2014).

[11] M. Brownnutt, M. Kumph, P. Rabl, and R. Blatt, Ion-trap measurements of electric-field noise near surfaces, Rev. Mod. Phys. **87**, 1419 (2015).

[12] E. E. Kleinsasser, M. M. Stanfield, J. K. Q. Banks, Z. Zhu, W.-D. Li, V. M. Acosta, H. Watanabe, K. M. Itoh, and K.-M. C. Fu, High density nitrogen-vacancy sensing surface created via He^+ ion implantation of ^{12}C diamond, Appl. Phys. Lett. **108**, 202401 (2016).

[13] E. Bauch, C. A. Hart, J. M. Schloss, M. J. Turner, J. F. Barry, P. Kehayias, S. Singh, and R. L. Walsworth, Ultralong Dephasing Times in Solid-State Spin Ensembles via Quantum Control, Phys. Rev. X **8**, 031025 (2018).

[14] R. O. Behunin, P. Kharel, W. H. Renninger, and P. T. Rakich, Engineering dissipation with phononic spectral hole burning, Nat. Mater. **16**, 315 (2017).

[15] G. Andersson, A. L. Oliveira Bilobran, M. Scigliuzzo, M. M. de Lima, J. H. Cole, and P. Delsing, Acoustic spectral hole-burning in a two-level system ensemble, npj Quantum Inform. **7**, 15 (2021).

[16] M. Scigliuzzo, L. E. Bruhat, A. Bengtsson, J. J. Burnett, A. F. Roudsari, and P. Delsing, Phononic loss in superconducting resonators on piezoelectric substrates, New J. Phys. **22**, 053027 (2020).

[17] Y. Tabuchi, S. Ishino, T. Ishikawa, R. Yamazaki, K. Usami, and Y. Nakamura, Hybridizing Ferromagnetic Magnons and Microwave Photons in the Quantum Limit, Phys. Rev. Lett. **113**, 083603 (2014).

[18] M. Pfirrmann, I. Boventer, A. Schneider, T. Wolz, M. Kläui, A. V. Ustinov, and M. Weides, Magnons at low excitations: Observation of incoherent coupling to a bath of two-level systems, Phys. Rev. Research **1**, 032023(R) (2019).

[19] D. Lachance-Quirion, Y. Tabuchi, A. Gloppe, K. Usami, and Y. Nakamura, Hybrid quantum systems based on magnonics, Appl. Phys. Express **12**, 070101 (2019).

[20] G. Woltersdorf, M. Kiessling, G. Meyer, J.-U. Thiele, and C. H. Back, Damping by Slow Relaxing Rare Earth Impurities in $Ni_{80}Fe_{20}$, Phys. Rev. Lett. **102**, 257602 (2009).

[21] L. Mihalceanu, V. I. Vasyuchka, D. A. Bozhko, T. Langner, A. Y. Nechiporuk, V. F. Romanyuk, B. Hillebrands, and A. A. Serga, Temperature-dependent relaxation of dipole-exchange magnons in yttrium iron garnet films, Phys. Rev. B **97**, 214405 (2018).

[22] H. Maier-Flaig, S. Klingler, C. Dubs, O. Surzhenko, R. Gross, M. Weiler, H. Huebl, and S. T. B. Goennenwein, Temperature-dependent magnetic damping of yttrium iron garnet spheres, Phys. Rev. B **95**, 214423 (2017).

[23] J. H. Van Vleck, Ferrimagnetic resonance of rare-earth-doped iron garnets, J. Appl. Phys. **35**, 882 (1964).

[24] P. W. Anderson, B. I. Halperin, and C. M. Varma, Anomalous low-temperature thermal properties of glasses and spin glasses, Philos. Mag. **25**, 1 (1972).

[25] J. L. Black and B. I. Halperin, Spectral diffusion, phonon echoes, and saturation recovery in glasses at low temperatures, Phys. Rev. B **16**, 2879 (1977).

[26] W. A. Phillips, Two-level states in glasses, Rep. Prog. Phys. **50**, 1657 (1987).

[27] H. Breuer, F. Petruccione, and S. Petruccione, *The Theory of Open Quantum Systems* (Oxford University Press, Oxford, 2002).

[28] N. V. Prokof'ev and P. C. E. Stamp, Theory of the spin bath, Rep. Prog. Phys. **63**, 669 (2000).

[29] J. T. Lin and Z. Y. Li, Microscopic model for the relaxation and excitation of localized spin waves, Phys. Status Solidi B **131**, 141 (1985).

[30] A. O. Caldeira, A. H. Castro Neto, and T. O. de Carvalho, Dissipative quantum systems modeled by a two-level-reservoir coupling, Phys. Rev. B **48**, 13974 (1993).

[31] J. Reichert, P. Nalbach, and M. Thorwart, Dynamics of a quantum two-state system in a linearly driven quantum bath, Phys. Rev. A **94**, 032127 (2016).

[32] H. Grabert and M. Thorwart, Quantum mechanical response to a driven Caldeira-Leggett bath, Phys. Rev. E **98**, 012122 (2018).

[33] H. Grabert, P. Nalbach, J. Reichert, and M. Thorwart, Nonequilibrium response of nanosystems coupled to driven quantum baths, J. Phys. Chem. Lett. **7**, 2015 (2016).

[34] C. Cohen-Tannoudji, J. Dupont-Roc, G. Grynberg, and P. Thickstun, *Atom-Photon Interactions: Basic Processes and Applications* (Wiley, New York, 1992).

[35] P. Meystre and M. Sargent, *Elements of Quantum Optics* (Springer, Berlin, 1991).

[36] H. J. Carmichael, Statistical Methods in Quantum Optics 1: Master Equations and Fokker-Planck Equations, *Theoretical and Mathematical Physics* (Springer, Berlin, 2010).

[37] B. R. Mollow, Power spectrum of light scattered by two-level systems, Phys. Rev. **188**, 1969 (1969).

[38] D. A. Holm, M. Sargent, and S. Stenholm, Quantum theory of multiwave mixing. IV. Effects of cavities on the spectrum of resonance fluorescence, J. Opt. Soc. Am. B **2**, 1456 (1985).

[39] K. Konthasinghe, J. Walker, M. Peiris, C. K. Shih, Y. Yu, M. F. Li, J. F. He, L. J. Wang, H. Q. Ni, Z. C. Niu, and A. Muller, Coherent versus incoherent light scattering from a quantum dot, Phys. Rev. B **85**, 235315 (2012).

[40] P. Grünwald and W. Vogel, Optimal squeezing in the resonance fluorescence of single-photon emitters, Phys. Rev. A **88**, 023837 (2013).

[41] H. S. Nguyen, G. Sallen, C. Voisin, P. Roussignol, C. Diederichs, and G. Cassabois, Ultra-coherent single photon source, Appl. Phys. Lett. **99**, 261904 (2011).

[42] T. Quang and H. Freedhoff, Spectrum of the one-atom dressed-state oscillator, Opt. Commun. **107**, 480 (1994).

[43] H. Freedhoff and T. Quang, Steady-state resonance fluorescence spectrum of a two-level atom in a cavity, J. Opt. Soc. Am. B **10**, 1337 (1993).

[44] S. Haroche and F. Hartmann, Theory of saturated-absorption line shapes, Phys. Rev. A **6**, 1280 (1972).

[45] B. R. Mollow, Stimulated emission and absorption near resonance for driven systems, Phys. Rev. A **5**, 2217 (1972).

[46] C. Cohen-Tannoudji and S. Reynaud, Dressed-atom description of resonance fluorescence and absorption spectra of a multi-level atom in an intense laser beam, J. Phys. B **10**, 345 (1977).

[47] C. Sánchez Muñoz, F. P. Laussy, E. del Valle, C. Tejedor, and A. González-Tudela, Filtering multiphoton emission from state-of-the-art cavity quantum electrodynamics, Optica **5**, 14 (2018).

[48] P. Heidler, C. M. F. Schneider, K. Kustura, C. Gonzalez-Ballestero, O. Romero-Isart, and G. Kirchmair, Observing non-Markovian effects of two-level systems in a niobium coaxial resonator with a single-photon lifetime of 10 ms, arXiv:2102.10016.

[49] F. Y. Wu, S. Ezekiel, M. Ducloy, and B. R. Mollow, Observation of Amplification in a Strongly Driven Two-Level Atomic System at Optical Frequencies, Phys. Rev. Lett. **38**, 1077 (1977).

[50] F. Nicacio, M. Paternostro, and A. Ferraro, Determining stationary-state quantum properties directly from system-environment interactions, Phys. Rev. A **94**, 052129 (2016).

[51] K. Kustura, C. C. Rusconi, and O. Romero-Isart, Quadratic quantum Hamiltonians: General canonical transformation to a normal form, Phys. Rev. A **99**, 022130 (2019).

[52] R. Simon, N. Mukunda, and B. Dutta, Quantum-noise matrix for multimode systems: U(n) invariance, squeezing, and normal forms, Phys. Rev. A **49**, 1567 (1994).

[53] S. Kosen, A. F. van Loo, D. A. Bozhko, L. Mihalceanu, and A. D. Karenowska, Microwave magnon damping in YIG films at millikelvin temperatures, APL Mater. **7**, 101120 (2019).